Contrib Mineral Petrol (2006) 151: 282–296
DOI 10.1007/s00410-005-0058-z

ORIGINAL PAPER

S. K. Simakov

Redox state of eclogites and peridotites from sub-cratonic upper mantle and a connection with diamond genesis

Received: 19 April 2005 / Accepted: 1 December 2005 / Published online: 26 January 2006

Abstract Pressure–Temperature- f_{O_2} conditions and fluid compositions estimated for mineral parageneses from inclusions in diamonds, diamond-bearing and diamond-free xenoliths using a garnet–clinopyroxene–silica oxygen barometer data indicate that the upper mantle is zoned, with a relatively oxidized lithosphere and a reduced asthenosphere. Calculations in the C–O–H system indicate that eclogite inclusions within diamonds and xenoliths have formed mainly in equilibrium with water-rich fluids.

Keywords Oxygen fugacity · Barometry · Mantle · Diamond genesis

Introduction

The oxidation state of the mantle has been a source of recent controversy. Thermodynamic calculations based on the olivine–orthopyroxene–spinel (O'Neill and Wall 1987) and olivine–orthopyroxene–garnet (Luth et al. 1990) equilibria along with measurement of Fe^{+3}/Fe^{+2} in basaltic glasses (Christie et al. 1986) support a relatively oxidized mantle, characterized by values of oxygen fugacity between fayalite–magnetite–quartz oxygen (FMQ) buffer and wustite-magnetite (WM) buffer. In contrast, the intrinsic oxygen-fugacity measurement (IOF) indicates more reduced values of f_{O_2}, near iron-wustite (IW) buffer (Ulmer et al. 1987). It has been suggested (Haggerty and Tompkins 1983) that the upper mantle is zoned with the depleted lithosphere being more reduced than the deeper, fertile portions of the asthenosphere. Taylor and Green (1989) and Ballhaus and Frost (1994) suggested an opposite view that the mantle consists of a relatively oxidized lithosphere and a reduced asthenosphere. Comparatively little attention has been paid to the role of oxygen fugacity in the diamond formation, which determines whether carbon exists either in the elemental form or remains complexed with oxygen in carbonates or in a gaseous species. Diamonds have formed in association with metal-silicate melts, traces of which have been noted in natural diamonds (Bulanova and Zayakina 1991). Such melts form at oxygen fugacities that corresponded to the IW buffer. From previous calculations based on the olivine–orthopyroxene–garnet equilibria, Simakov (1998) argued that diamonds with peridotite inclusions were formed under the reducing conditions corresponded to IW buffer. On the other hand, the presence of carbonate inclusions and solid CO_2 in diamonds would indicate a more oxidizing environment (Bulanova and Pavlova 1987; Schrauder and Navon 1993), corresponding to the QFM buffer. Schrauder and Navon (1993) suggested that the carbon for the formation of the diamond might have come from a partial reduction of CO_2 itself. From the composition of phases in spinel peridotites it follows that f_{O_2} may vary by five log units in the lithosphere under the ancient cratons (Ballhaus 1993). The oxidation state of garnet lherzolites and eclogites has not been as extensively studied as that of spinel lherzolites.

Calibration of garnet–clinopyroxene–silica oxygen barometer

The oxidation state of the mantle can be estimated by redox reactions involving iron-bearing minerals. Commonly, the phase containing ferric iron is the spinel, but it is possible to calibrate a garnet–clinopyroxene–silica barometer based on the solubility of Fe^{+3} in garnets. Zhang and Saxena (1991) proposed to use the reactions of the garnet–clinopyroxene–quartz equilibrium for skarns with coexisting andradite and hedenbergite. Another reaction was proposed by Simakov (1993) for mantle eclogites:

Communicated by T. L. Grove

S. K. Simakov
Geological Department, St Petersburg University,
7/9 Universitetskaya Nab., St. Petersburg 199034, Russia
E-mail: simakov@ap1250.spb.edu

$$\underset{\text{Andr}}{2Ca_3Fe_2Si_3O_{12}} + \underset{\text{Fs}}{Fe_2Si_2O_6} + \underset{\text{Qu(Cs)}}{4SiO_2} \Rightarrow \underset{\text{Hed}}{6CaFeSi_2O_6} + O_2 \quad (I)$$

For this reaction, the oxygen-fugacity value is expressed as:

$$\log f_{O_2} = -\Delta G^P_T/2.303RT - \alpha^6_{\text{Hed}}/(\alpha^2_{\text{Andr}}\alpha^4_{SiO_2}\alpha_{\text{Fs}}), \quad (1)$$

$\Delta G^P{}_T$ was calculated from the thermochemical data compiled by Kuskov and Fabrichnaya (1990) and Moecher et al. (1988) (Table 1). Clinopyroxene-activity models are calculated in accordance with the formulas:

$$\alpha_{\text{Hed}} = \gamma_{\text{Hed}}Ca^{M2}Fe^{M1}Si^2, \quad (2)$$
$$\alpha_{\text{Fs}} = \gamma_{\text{Fs}}Fe^{M2}Fe^{M1}Si^2, \quad (3)$$

where:

$$M1 = Fe^{M1} + Mg^{M1} + Ti + Cr + Fe^{+3} + Al^{M1},$$
$$M2 = Fe^{M2} + Mg^{M2} + Ca + Mn + Na + K,$$
$$Al^{M1} = X_{Al} - Al^{IV},$$
$$Al^{IV} = 2 - X_{Si},$$
$$Si = X_{Si}/2.$$

this clinopyroxene model was tested by comparing it with the experimental data of omphacitic clinopyroxenes (Simakov 2005) and hedenbergite–jadeite solutions (Fig. 1) (Perchuk and Aranovich 1991). The andradite activity ($\alpha_{\{\text{Andr}\}}$) is calculated using the multi-component solid-solution model in garnet (Simakov 1998):

$$\log \alpha_{\text{Andr}} = (G^e_{\text{Andr}_{\text{I - II}}} + 3G^e_{\text{Andr}_{\text{I}}} + 2G^e_{\text{Andr}_{\text{II}}})/RT + \log X^3_{Ca}X^2_{Fe} + 3. \quad (4)$$

Non-ideal mixing on the dodecahedral sites ($G^e_{\text{Andr}_{\text{I}}}$) is treated by an asymmetric sub-regular solution model with the formulation given by Moecher et al. (1988). Non-ideal mixing on the octahedral sites ($G^e_{\text{Andr}_{\text{II}}}$) was treated with a symmetric regular solution model with the interaction parameters listed in Table 4. Reciprocal solid-solution effects in the garnets (Wood and Nicols 1978) were accounted for with the exchange reactions:

$$\underset{\text{Pyr}}{Mg_3Al_2Si_3O_{12}} + \underset{\text{Andr}}{Ca_3Fe_2Si_3O_{12}} = Mg_3Fe_2Si_3O_{12} + \underset{\text{Gross}}{Ca_3Al_2Si_3O_{12}} \quad (II)$$

$$\underset{\text{Andr}}{Ca_3Fe_2Si_3O_{12}} + \underset{\text{Alm}}{Fe_3Al_2Si_3O_{12}} = \underset{\text{Ski}}{Fe_3Fe_2Si_3O_{12}} + \underset{\text{Gross}}{Ca_3Al_2Si_3O_{12}} \quad (III)$$

$$\underset{\text{Pyr}}{Mg_3Al_2Si_3O_{12}} + \underset{\text{Uvar}}{Ca_3Cr_2Si_3O_{12}} = \underset{\text{Knor}}{Mg_3Cr_2Si_3O_{12}} + \underset{\text{Gross}}{Ca_3Al_2Si_3O_{12}} \quad (IV)$$

$$\underset{\text{Uvar}}{Ca_3Cr_2Si_3O_{12}} + \underset{\text{Alm}}{Fe_3Al_2Si_3O_{12}} = \underset{\text{Fe - Knor}}{Fe_3Cr_2Si_3O_{12}} + \underset{\text{Gross}}{Ca_3Al_2Si_3O_{12}} \quad (V)$$

The scheme of element distribution from M1 and M2 position is taken from Wood and Banno (1973). The activity coefficients of the clinopyroxene minerals was modeled by assuming the clinopyroxene as an asymmetrical solid-solution model. On the M1 and M2 positions, the parameters of interactions were taken from the papers listed in Table. 2 and 3. The precision of

The Gibbs free energy values of these reactions are listed in Table 4. This model can be applied to the peridotite parageneses by calculating the activity of silica in accordance with the thermodynamic model of olivine–orthopyroxene equilibrium in the upper mantle (O'Neill and Wall 1987) by the reaction:

Table 1 Gibbs free energy, entropy, molar volume and entropy coefficients of the phases involved in the thermodynamic calculations

Mineral	$\Delta G°_{298}$ (kJ/mol)	$S°_{298}$ (J/mol K)	$V°_{298}$ (cc/mol)	A	B	C	D	E
Andradite	−5,413.2	316.82	131.67	470.395	46.903	63.743	−2,765.6	
Ferrosilite	−2,232.4	191.64	63.98	232.99	30.402	32.318	−1372.6	
Hedenbergite	−2,677.7	173.59	67.85	214.116	48.359	24.698	−1,262	
Quartz (α)	−856.6	41.46	22.69	73.448	0.782	15.376	436.1	
Oxygen (O_2)	0.0	205.04		20.15	28.078	2.065	−1.772	4.172

The thermochemical data were taken from: Moecher et al. (1988). The $\Delta G^P{}_T$ of α-Quartz ⇒ Coesite transition is calculated in accordance with the equation given in Kuskov and Fabrichnaya (1990)

Table 2 Data of interaction parameters on M2 clinopyroxene position (in J/mole, $T°$ *K*, *P*—kbar)

(M2)	Ca–Mg	Mg–Ca	Ca–Fe	Fe–Ca	Mg–Fe	Ca–Na	Na–Ca	Mg(Fe)–Na
[a]	31,216−6.1 *P*	25,484+8.12 *P*	20,697−2.35 *P*	16,940+5.9 *P*				
[b]					−2,172	31,120	16,707	
[c]								
[d]								−24,000

The data were taken from:
[a] Lindsley (1981)
[b] Lindsley et al. (1981)
[c] Mukhopadhyay (1991)
[d] Simakov (2005)

Table 3 The gata of interaction parameters on M_1 clinopyroxene position (in J/mole, $T°$ *K*, *P*—kbar)

(M1)	Mg–Fe	Fe–Mg	Mg(Fe)–Cr	Al–Cr	Mg(Fe)–Al	Al–Mg(Fe)
[c]	3,978					
[d]					42,000−10.63 *T*	−1,000
[e]			18,481	20,000		

[e] Girnis and Grutter (2003), another reference the same as in Table 2

$$\underset{\text{Fo}}{Mg_2SiO_4} + \underset{\text{Qu(Cs)}}{SiO_2} \Rightarrow \underset{\text{Enst}}{2MgSiO_3} \qquad (V)$$

This model can be also applied to the garnet–orthopyroxene–clinopyroxene parageneses. We can calculate the composition of fictive olivine in accordance with the thermodynamic model of olivine–orthopyroxene equilibrium in the upper mantle (Seckendorff and O'Neill 1993) by the reaction:

$$\underset{\text{Fa}}{0.5\ Fe_2SiO_4} + \underset{\text{Enst}}{MgSiO_3} = \underset{\text{Fo}}{0.5Mg_2SiO_4} + \underset{\text{Fs}}{FeSiO_3} \qquad (VII)$$

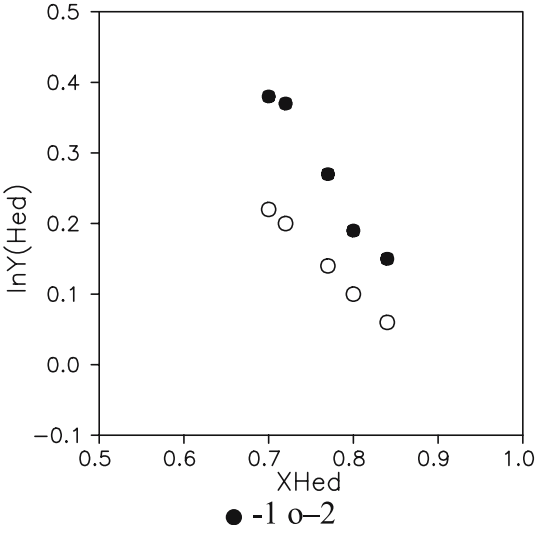

Fig. 1 A comparison of the experimental data of Hed–Jd solution (Perchuk and Aranovich 1991) (1) with calculated ones (2) by our Cpx model

Careful studies of eclogites by Sobolev et al. (1999a, 2000) show the presence of coesite inclusions in eclogite diamonds from kimberlites and lamproites. This implies that we could apply the reaction (I) to mantle eclogite parageneses by taking the activity of SiO_2 to be 1 (Nakamura and Banno 1997). This model can be also applied to the Si-undersaturated eclogite parageneses. We can use the fictive minal of SiO_2 with activity equal to 1. Because ferric iron is so low in garnet, the garnet–clinopyroxene–silica–oxygen barometer requires a careful measurement of Fe^{+3}/Σ Fe in garnet and clinopyroxene. There are only two analytical methods commonly used to determine Fe^{+3}/Σ Fe directly, Mossbauer spectroscopy, and wet chemistry. It has been common practice to use the crystal chemistry of silicate phases analyzed by the electron microprobe (EMP) to calculate the Fe^{+3} of a mineral. Several attempts have been made to compare and correlate the measured and calculated Fe^{+3}/Σ Fe contents in silicates from upper mantle xenoliths. Luth et al. (1990) stated that for peridotite minerals (garnet, olivine, clino-, and orthopyroxene) the values of Fe^{+3}/Σ Fe measured by the Mossbauer technique were significantly different from those calculated from the EMP analyses. Ballhaus et al. (1991) have demonstrated that stoichiometric Fe^{+3} in spinel agrees well with the ones measured by Mossbauer spectroscopy. Canil and O'Neill (1996) showed that the level of imprecision in Fe^{+3} determined from EMP analyses is related to the total Fe content, and increases in the order: spinel < garnet < clinopyroxene. McCammon et al. (1998) and Sobolev et al. (1999b) used the Mossbauer milliprobe to determine Fe^{+3}/Σ Fe in eclogite garnet and clinopyroxene from George Creek diamonds and Udachnaya kimberlite. Woodland and Peltonen (1999), Woodland and Koch (2003), and McCammon and Kopylova (2004) used the Mossbauer milliprobe to determine Fe^{+3}/Σ Fe in peridotite garnet

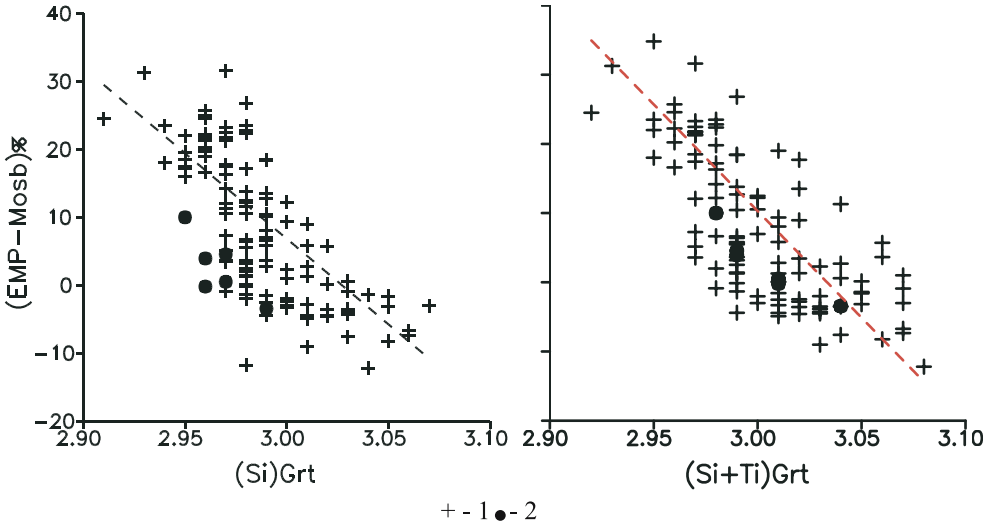

Fig. 2 The relationship between Si and Si + Ti contents and differences between EMP and Mossbauer Fe^{+3}/Σ Fe for the upper mantle garnet (1, peridotite garnets; 2, eclogite garnets). Analyses for the calculation were taken from: Canil and O'Neil (1996), Luth et al. (1990), McCammon and Kopylova (2004), McCammon et al. (1998), Sobolev et al. (1999), Woodland and Koch (2003)

Table 4 The data of the garnet-interaction parameters on the octahedral site ($G^e_{\{Andr\{II\}}$) and between dodecahedral and octahedral sites expressed in the Gibbs free energy of the exchange reactions (in J/mole, T° K, P—kbar)

$G^e_{Andr_{II}}$			$G^e_{Andr_{I-II}}$			
W_{Al-Cr}	W_{Al-Fe}	W_{Cr-Fe}	II	III	IV	V
2,508	3,700	1,267	25,080	40,200−7 P	122,181−49.7 T	106,903−43.45 T

The data were taken from: Aranovich (1991), Luth et al. (1990), Woodland and O'Neill (1993)

from Southern Africa, Finnish and Canadian kimberlites. Sobolev et al. (1999b) stated that the accuracy of the ferric iron estimate depends on the accuracy of the silica determination. A comparison of the Fe^{+3}/Σ Fe values calculated by Schumacher's (1991) model with those determined by Mossbauer techniques for mantle garnets shows the correlation between the error in garnet Fe^{+3}/Σ Fe determination and Si and Si + Ti contents (Fig. 2). The lowest error lies in the range of 3.03 ± 0.02 f.u. $(Si + Ti)_{Grt}$ (Fig. 2).

Uncertainties of the calculated oxygen fugacity result from uncertainties in the activity model of the minerals involved and the calculated pressure and temperature. At temperatures more than 1,100°C, oxygen fugacity on 70% and more depends upon the mineral activities and only on 30% or less upon the P–T parameters. Otherwise, at low temperatures the $f_{\{O2}$ on 70% depends upon P–T parameters and only on 30% or less upon the mineral activities. The andradite minal is the 45–55% part of the total mineral activity, the hedenbergite one is 30–35%, the ferrosilite one is 10–15% and the silica one is only 1–3% (for peridotite parageneses). The andradite activity coefficient is 10–15% part of the total mineral activity, the hedenbergite one is 5–7% and ferrosilite and silica ones are by 1–3%. The 4 kJ/mole error in the free energy of formation of andradite yields an uncertainty of about ± 0.1 log f_{O_2}. The reciprocal terms in the f_{O_2} calculation are typically in the order of 0.3 log units while the uncertainty in Fe^{+3} content of garnet leads to 0.5 log units in f_{O_2} uncertainty. The uncertainty in Fe^{+3} content of clinopyroxene leads to 0.5 log units in f_{O_2} uncertainty too. Assuming a normal distribution of these errors implies a total uncertainty of ± 0.8 log units

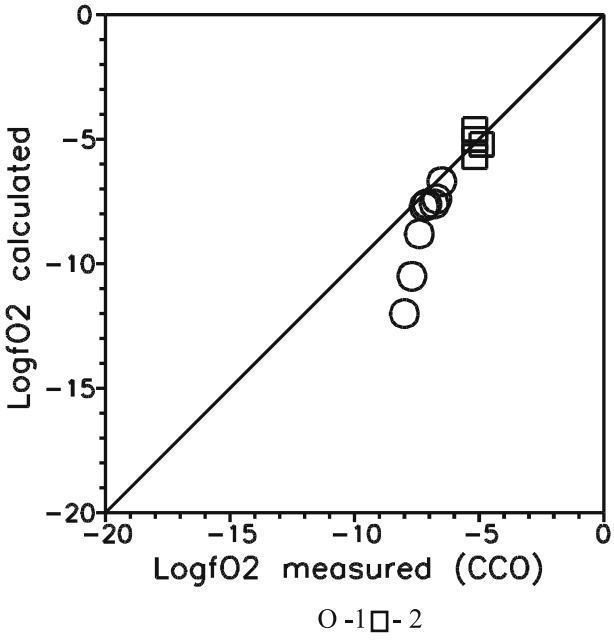

Fig. 3 The difference between the f_{O_2} values calculated by the equilibrium (I) and measured for synthesized nearly CCO buffer eclogites [1, Yaxley (1999)] and carbonatized peridotites [2, Ryabchikov et al. (1993)]

in f_{O_2} for our sensor. The accuracy of garnet–clinopyroxene–silica oxygen barometer was tested on the experimental data of garnet–clinopyroxene assemblages synthesized in the carbonate-bearing eclogite system at 30–35 kb and 700–900°C and on the garnet–two-pyroxene–olivine assemblages synthesized in the peridotite system at 50 kbars and 1,400–1,550°C with the oxygen fugacity controlled by the CCO buffer (Ryabchikov et al. 1993; Yaxley 1999) (Fig. 3). Fe^{3+} were calculated for the garnets with $(Si+Ti)_{Grt}$ of 3.0 ± 0.02 f.u. from the EMP analyses. As can be seen from Fig. 3, oxygen fugacities calculated from equilibrium (I) are in fair agreement with oxygen fugacities measured with the CCO sensor. The only data which lie outside the quoted uncertainties could be from those experiments in which garnet and clinopyroxene were not in exchange equilibrium. Accuracy of the barometer also was tested on the garnet–spinel lherzolites by comparing the oxygen fugacity calculated from the garnet–clinopyroxene–silica equilibrium with those from the olivine–orthopyroxene–spinel equilibrium. These calculations are correct when the minerals of the paragenesis are in mutual equilibrium. Yakutian kimberlitic garnet–orthopyroxene–clinopyroxene–olivine–spinel lherzolite was chosen for the oxygen-fugacity calculations. The difference between garnet–orthopyroxene, spinel–olivine, clinopyroxene–orthopyroxene, two-pyroxene and garnet–olivine thermometers did not exceed 50°C (Table 5). Accuracy of the barometer was also tested on the garnet lherzolites with Mossbauer garnet and clinopyroxene data by the comparing the oxygen fugacity calculated from the equilibrium (I) with those from the olivine–orthopyroxene–garnet sensor of Gudmudson and Wood (1995) with an accuracy of ± 0.6 log f_{O_2} units. The parageneses were chosen for oxygen- fugacity calculations by the procedure described above. The difference between garnet–orthopyroxene, clinopyroxene–orthopyroxene, two-pyroxene and garnet–olivine thermometers did not exceed 155°C. Calculated f_{O_2} values for South African, Canadian, and Yakutian parageneses coincide with the calculations for the same analyses done with using the Gudmundson and Wood (1995)

Table 5 Garnet–spinel–orthopyroxene–clinopyroxene–olivine paragenesis separated for P–T-$f_{\{O2}$ calculations

Sample	NG85	H84	NW79	B91	Ai93	T98	$\Delta(f_{O_2})_1$	$\Delta log(f_{O_2})_2$
Yakutian xenolith								
Uv-624	42.68	847	856	824	874	847	−2.7	−2.1

NG85, Grt–Opx barometer of Nickel and Green (1985) (in kbar); H84, Grt–Opx thermometer of Harley (1984); NW79, Grt–Ol thermometer of O'Neill and Wood (1979); Ai93, Grt–Cpx thermometer of Ai (1993); T98, Cpx–Opx thermometer of Taylor (1998) (in °C). $\Delta log(f_{O_2})_1$, calculated values by garnet–clinopyroxene–silica barometer; $\Delta log(f_{O_2})_2$, values obtained by spinel–orthopyroxene–olivine barometer of Ballhaus et al. (1991) with Taylor and Grenn's (1991) correction for high-chromium spinels at the same pressures and temperatures relative to the QFM buffer of Frost (1991). For f_{O_2} calculations P–T parameters obtained from garnet–orthopyroxene, thermobarometers of Harley (1984) and Nickel and Green (1985) were used. Analyses for the calculations were taken from Pokhilenko et al. (1991)

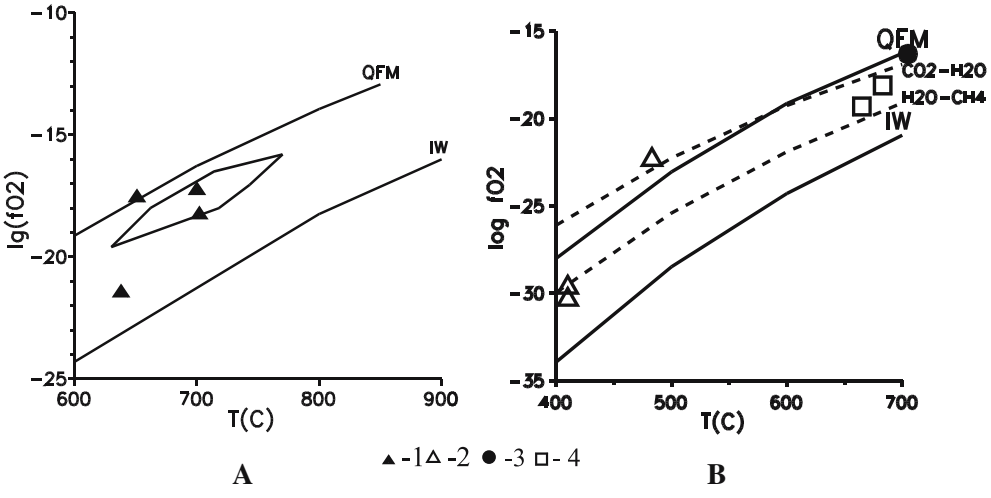

Fig. 4 A comparison of the oxygen fugacities calculated using our sensor (1, Johnston and Essene 1982; Spear and Markussen 1997) with those, obtained by Lamb and Valley (1984) using the Mgt–Ilm sensor (*solid curve* between QFM and IW) for Andirondack complex (**a**), results of oxygen-fugacity calculations for Voltri Massif [2, Messiga and Scambelluri (1991)], Saulpian [3, Mottana et al. (1968)] eclogites and Southern Karnataka (Indian) metamorphites [4, Hansen et al. (1984a); Janardan et al. (1982)] (**b**). For temperature estimation, the thermometer of Ai (1993) was used at $P = 7$ kbar (*upper dashed line*—CCO buffer, *lower dashed line*—H_2O–CH_4—fence)

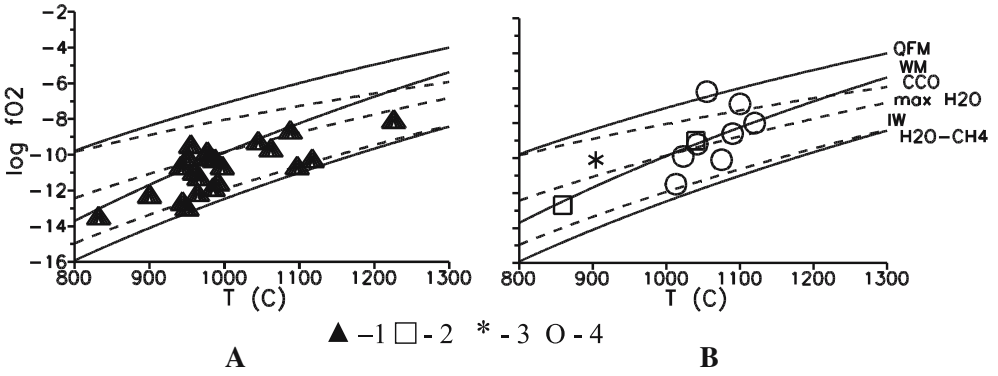

Fig. 5 The results of oxygen-fugacity calculations for South African and Yakutian peridotite garnet–two-pyroxene–olivine parageneses (see Appendix 1) with using Mossbauer data (1) (**a**) and for Yakutian (2, diamond bearing; 3, diamond-free); Namibian and Lesotho (4) peridotites with using EMP data (**b**) with using the garnet–clinopyroxene–silica oxygen barometer at 45 kbar

equilibrium (see Appendix 1). I conclude, therefore, that equilibrium (I), with free energy and the activity terms discussed above should, in general, yield the oxygen fugacity values to within ±0.8 log units.

The oxygen barometer can also be applied to crustal eclogites using the model of Fe and Mg distribution on the M1 and M2 sites of clinopyroxene in accordance with the formulation of Dal Negro et al. (1982). The sensor was applied to crustal eclogitic and granulitic rocks from different metamorphic complexes. Andirondack complex in northern United States is one of the well-studied metamorphic complexes in the world (Johnston and Essene 1982; Spear and Markussen 1997). It was applied to olivine-bearing metagabbros and granulites from the Adirondack and the obtained f_{O_2} values were compared with those calculated for the same rocks by the magnetite–ilmenite oxybarometer (Lamb and Valley 1984) (Fig. 4a). From another side, the results were compared to the compositions of fluid inclusions that were measured in the rocks. For the Voltrian Group eclogites, the calculated f_{O_2} values correspond to or are above the QFM buffer (Fig. 4b), for Southern Karnataka (India) granulites and charnokites, the calculated f_{O_2} values correspond to the QFM and WM buffers (Fig. 4b), in agreement with the water and water–carbon dioxide compositions of fluid inclusions in these rocks (Mottana et al. 1968; Messiga and Scambelluri 1991; Hansen et al. 1984b).

Results and discussion

Pressure–Temperature f_{O_2} parameters were calculated for inclusions within diamonds, diamond-bearing and diamond-free xenoliths from Australia, South Africa, and Yakutia using EMP and Mossbauer Fe^{+3} analyses for garnet and clinopyroxene. For the calculations based on EMP analyses, only the garnet with $(Si+Ti)_{Grt}$ of 3.03 ± 0.02 f.u. was used (see Appendices 1, 2). For the eclogite garnet–clinopyroxene parageneses, the

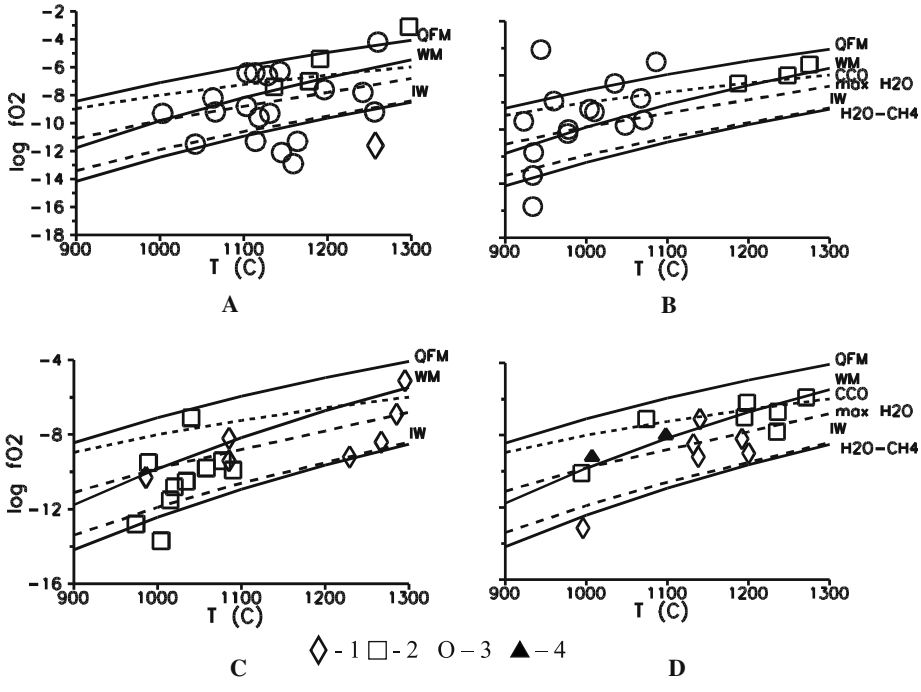

Fig. 6 The results of oxygen-fugacity calculations for Roberts Victor (**a**), Koidu and diamond-bearing Finnish (**b**), Mir (**c**), and Udachnaya (**d**) eclogites at 45 kbar (see Appendix 2). (1, diamond inclusion; 2, diamond-bearing eclogites; 3, xenoliths, and 4, diamond-bearing xenoliths of Udachnaya pipe, calculated with using Mossbauer data). [*solid lines*: *QFM* quarts–fayalite–magnetite, *WM* wustite–magnetite, *IW* iron–wustite (Frost 1991), *dashed lines*: CCO buffer—correspond to upper limit of diamond stability in C–H–O system, max H_2O—correspond to the reaction X, H_2O–CH_4—correspond to the lower boundary of water-rich ($X_{H_2O} > 0.5$) fluids] (see Simakov 1998)

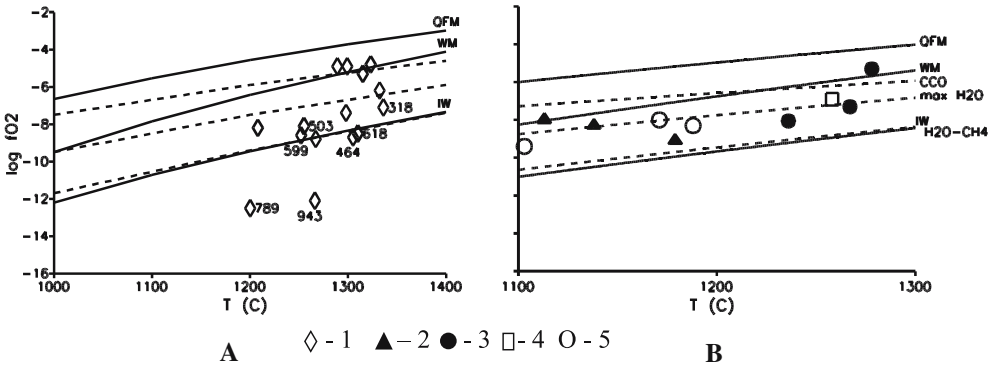

Fig. 7 The results of oxygen-fugacity calculations for eclogite diamond inclusions from Premier (1) (**a**) George Creek (2, Mossbauer data), Argyle (3), Guinea (4) and Venezuela (5) (**b**) at 50 kbar (see Appendix 2). For Premier and Finsh diamonds, the data of nitrogen content of Deines's et al. (1989) in ppm is plotted

temperature was estimated using the garnet–clinopyroxene thermometer of Ellis and Green (1979). The peridotite garnet–two-pyroxene–olivine parageneses were chosen during the procedure described above.

Fluid compositions for eclogite and peridotite parageneses were estimated as a function of P, T and f_{O_2} with the assumption that they were free carbon-saturated. The fluid composition in equilibrium with diamond was calculated in accordance with the scheme described in Simakov (1998). In the C–H–O system, the upper limit of carbon stability in terms of oxygen fugacity corresponds to the reactions of the CCO buffer:

$$CO_2 \rightarrow C + O_2, \qquad (VIII)$$
$$CO \rightarrow C + 0.5O_2. \qquad (IX)$$

In the mantle, however,the CCO buffer is only of theoretical importance. In C–O–H system, diamond does not impose a lower f_{O_2} limit. One may be included to place a common lower limit near an f_{O_2} defined by the equilibrium:

$$CH_4 + O_2 \rightarrow C + 2H_2O, \qquad (X)$$

below, which the partial pressures of CH_4 and H_2 exceed the partial pressures of CO_2 and CO and main part of the free carbon transfers to the methane.

Most of the peridotitic diamond-bearing and diamond-free xenoliths lie at oxygen fugacities below those of the CCO buffer (Fig. 5). Most of the eclogitic inclusions within diamonds also equilibrated at conditions below those of the CCO buffer, near WM (Figs. 6, 7). The results show that at these oxygen fugacities, the average calculated eclogite fluid compositions are water-rich [real apparent error of the Grt–Cpx–Qu(Cs) sensor (± 0.8 log units in f_{O_2}) could not have great effect on the average results] and close to the average composition of the gaseous inclusions in natural diamonds (see Fig. 8).

Calculated P–T- f_{O_2} results obtained for peridotite parageneses show that oxygen fugacity in the upper mantle mainly decreases with the depth (Fig. 9). It confirmed the conclusion of Taylor and Green (1989) that the upper mantle under the ancient cratons is zoned and consists of relatively oxidized lithosphere and reduced asthenosphere. Reduction and the fluid H_2O/CO_2 ratio increase with increasing depth (Fig. 5), which agrees with the experimental data in the carbonated peridotite-fluid system (Wyllie 1977) and with the thermochemical computation of oxidation state of the mantle (Saxena 1989).

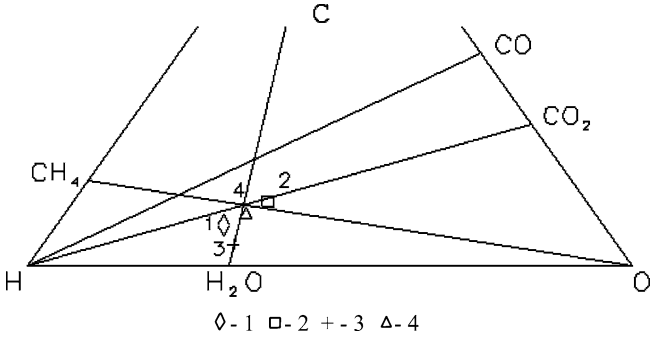

Fig. 8 Average compositions of the calculated fluids for African parageneses: 1, eclogite inclusions from diamonds (average of 40 analyses); 2, eclogite xenoliths (average of 66 analyses); 3, peridotite xenoliths (average of 32 analyses) ; 4, fluid extracted from South African, Brazilian, and USA diamonds (average of 36 crystals) (Giardini and Melton 1975). Analyses for calculations were taken from Appendices 1 and 2

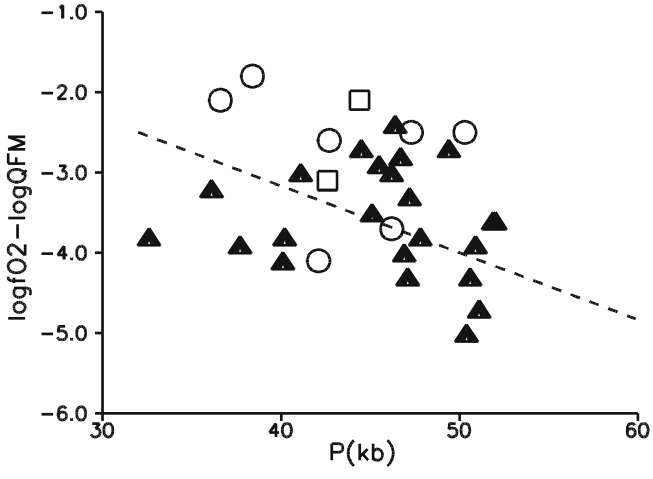

Fig. 9 Log $(f_{O_2})_{calc}$–log(QFM) dependencies for peridotites on the pressure (symbols—the same as on Fig. 5)

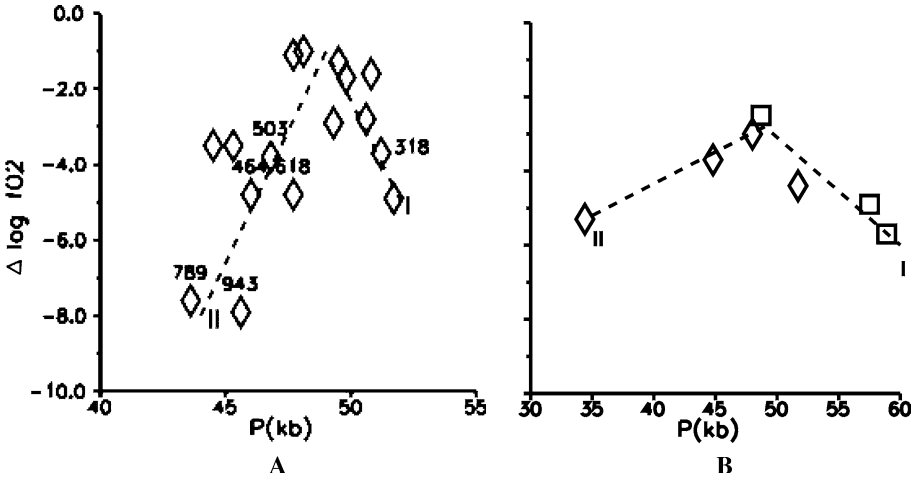

Fig. 10 $\Delta log(f_{O_2}) = log(f_{O_2})_{calc}$-log(QFM) dependencies for Premier (**a**) and Udachnaya (**b**) eclogites on the pressure (symbols—the same as on Figs. 6, 7). I and II are the limbs of the crystallization. The pressure was calculated on the basis of CaTs barometer (Simakov and Taylor 2000)

Calculated *P–T*- f_{O_2} results obtained for eclogite parageneses with using Grt–Cpx barometer of Simakov and Taylor (2000) show different trends for oxygen fugacity in the upper mantle at real apparent errors of the Grt–Cpx–Qu(Cs) sensors in ±0.8 log units of f_{O_2} and in 5 kbars of pressure. *P–T*- f_{O_2} results obtained for eclogite inclusions within diamonds for Premier and Udachnaya pipes show a distinct kink in the oxygen-fugacity trajectory (Fig. 10 limbs I and II). At depths lower than 150 km, the oxygen fugacity decreases with depth (limb I). Between the level of 100–150 km, there is a tendency for oxygen fugacity to rise with increasing depth (limb II). At both the localities, maximum of oxygen fugacity corresponds to a depth of 140–160 km. From these data, we can infer that there are two main levels of diamond formation in the upper mantle: (1) crystallization of initial asthenosphere diamonds under very low- f_{O_2} conditions at depths of 160–180 km; (2) diamond crystallization and growth in equilibrium with water- and carbon dioxide-rich fluids in the lithosphere at the depths of 130–160 km. In other words, we can conclude that the asthenospheric diamonds form at high pressures, low-oxygen fugacities, and CH_4-rich fluids, whereas the lithospheric diamonds form at lower pressures, higher oxygen fugacities, and in H_2O–CO_2-rich fluids. The oxygen fugacity mainly decreases from the oxidized lithosphere to the reduced asthenosphere.

Mantle model

The observed oxygen-fugacity trajectory can be explained by the hot plume uplifting under the central parts of cratons (Fig. 11). The plume could be intruded from the deep levels of the asthenosphere to the lithosphere–asthenosphere boundary or the lower parts of the lithosphere, which contained subducted

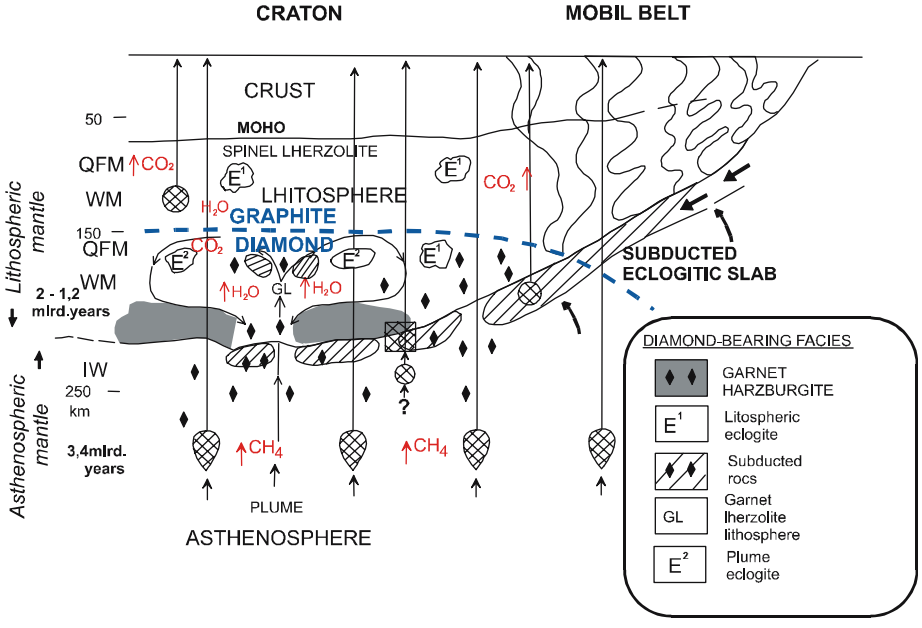

Fig. 11 Hypothetical cross-section of an Archean craton and adjacent cratonized mobile belt in accordance with Haggerty (1986) and Mitchell (1991) models, showing the variation of the oxygen-reduction conditions in the upper mantle

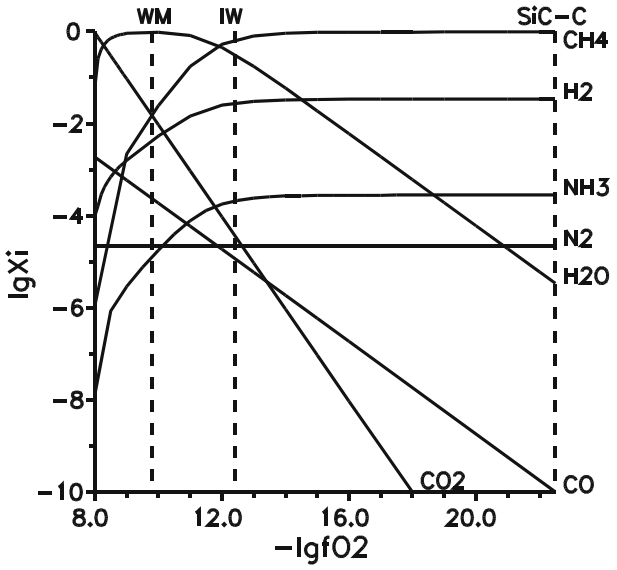

Fig. 12 The result of calculation of O–H–N–C system up to SiC–C boundary [by the data of Woerman and Rosenhauer (1985)] at $P = 45$ kbar and $T = 1{,}000$°C and $P_{N_2} = 1$ bar. (Calculations of γ_i of the gases were performed by the methods of Belonoshko and Saxena (1992), who fit their expressions to experimental data for molar volume of these components up to 6,090° K and 80 GPa)

rocks with carbonates. The plume melts could contain ancient harzburgite diamonds formed in reduced conditions in the asthenosphere from metal-silicate melts. The plumes could contact with lithosphere subducted rocks (Taylor and Green 1989). Under the process of heating, the reaction Dol + Coes = liq + CO_2 would be crossed, releasing CO_2. This is supported by the isotopic data, which shows that light crustal carbon participated in the formation of eclogite diamonds (Deines et al. 1987). From this model, it follows that the part of the eclogitic diamonds could be formed as a result of the interactions between CO_2 released during heating and the reduced upper mantle fluid components. As a result, the initial garnet peridotites could be melted forming carbon–silicate melts and water–carbon dioxide fluids. Diamonds could be formed from these melts (Pal'yanov et al. 1999), the traces of which were founded in natural diamonds (Schrauder and Navon 1993). The Mitchell (1991) reconstruction of the lithosphere and asthenosphere profile indicates that eclogites can form during the contact of the plume magmas with the garnet lherzolite part of lithosphere or with the remnants of ancient subducted rocks (Mitchell 1991) (see Fig. 11). Crystallization of the diamonds with lherzolite and eclogite parageneses in equilibrium with H_2O–CO_2-rich fluids could take place from carbon–silicate melts as a result of these processes.

At the levels of 130–160 km, there was a peak of the CO_2 releasing and as a result, there is a maximum of the eclogite parageneses oxidation, which is two to three log units higher than the peridotite trend at the same depths (see Figs. 9, 10). Deines et al. (1989) noted the tendency for the nitrogen content of eclogitic Premier diamonds to decrease with temperature of formation. It follows that the nitrogen content decreases with temperature and with increasing oxygen fugacity (Figs. 7, 10a—limbs I and II). Sobolev et al. (1966) proposed that nitrogen was included into the diamond structure at a deep-seated stage of degassing of the mantle by the reaction, which decreases the decomposition of NH_3 to H^- and N^{+3} .

$$NH_3 \rightarrow N + 3 + 3H^-. \qquad (XI)$$

The problem of nitrogen presence in the upper mantle was discussed in the previous paper (Simakov 1998). From the calculations and mineralogical data, it follows that nitrogen could be present in the upper mantle in the forms of N_2 and NH_3 gases. The calculations in C–H–O–N system shows that ammonia concentration must be inversely proportional to CO_2 (Fig. 12). This agrees with the tendency for nitrogen content of the Premier diamonds to decrease with increasing oxygen fugacity or temperature.

Conclusions

The calculations above show that f_{O_2} in the lithospheric upper mantle under the Archean cratons varies over a range of five to six log units, which agrees with the previously obtained results for spinel and garnet peridotite xenoliths (Ballhaus 1993; Simakov 1998; Woodland and Koch 2003). These results indicate that the upper mantle is zoned and the degree of its reduction increases with depth from lithosphere to asthenosphere.

From the calculations it follows that mantle eclogite xenoliths are more oxidized than the peridotite ones (Fig. 8). It agrees with the experimental data of Pokhilenko and Tomilenko (2001). It is known that the peridotite diamond inclusions are more ancient than eclogitic ones (Richardson et al. 1993), which is why eclogitic diamonds are enriched by light crustal carbon relative to the peridotitic ones (Galimov 1984; Deines et al. 1987).

Diamond preservation in the mantle depends upon the oxygen fugacity. The optimum conditions for diamond growth and preservation in C–H–O system correspond to those where a water-rich fluid would be stable (if the upper mantle is be fluid-saturated), which agrees with the previously obtained results for peridotite xenoliths (Ballhaus 1993; Simakov 1998).

Acknowledgments The author wish to express his gratitude to Drs. R.F.Frost, G.P.Bulanova, D.Canil, C.A.McCammon, M.G.Kopylova, J.L.R.Touret, C. Smith, and N.V.Sobolev for their constractive criticism, valuable advice and interest in my work. The research was supported by the RF President Program on Leading Scientific Schools (grant No. 1645.2003.5) and RFFI grant No 06-05-64183-A

Appendix 1

Table 6 Garnet–orthopyroxene–clinopyroxene–olivine parageneses chosen for P–T- f_{O_2} calculations

Sample	NG85	H84	NW79	Ai93	T98	$\Delta log(f_{O_2})_1$	$\Delta log(f_{O_2})_2$
South African xenoliths							
FRB1350[a]	33	880	857	725	746	−3.6	−3.0
89–719[a]	47	1,130	1,225	1,120	1,121	−4.2	−4.6
VBD1140[a]	40	937	910	964	897	−3.6	−3.1
BD1150[a]	41	944	958	1,024	1,024	−2.8	−2.7
FRB909[a]	52	1,274	1,348	1,380	1,343	−3.7	−3.6
FRB921[a]	38	1,000	1,009	1,050	1,000	−3.8	−3.4
Canadian slave xenoliths							
10–12a[a]	36	788	726	749	771	−2.9	−2.7
22–5[a]	48	970	842	976	909	−1.9	−3.3
25–9[a]	40	875	837	880	813	−3.3	−4.1
14–107[a]	46	958	968	1,010	995	−2.5	−2.4
40–11[a]	48	99	1,018	1,060	1,052	−3.1	−3.8
21–6[a]	51	1,024	1,025	1,075	1,110	−4.8	−4.3
21–4[a]	46	965	967	1,043	1,021	−3.3	−3.5
21–3[a]	48	999	970	1,045	1,022	−4.6	−4.0
22–7[a]	53	1,030	1,040	1,170	1,120	−3.4	−3.6
41–1[a]	50	967	960	1,100	1,053	−3.2	−2.7
23–5[a]	45	1,045	1,074	1,180	1,190	−2.6	−2.7
9–10[a]	47	988	1,013	1,143	1,129	−2.5	−3.0
41–3[a]	47	1,101	1,112	1,245	1,190	−2.5	−2.8
Lesotho xenoliths							
133	45	1,052	1,064	1,044	1,016	0.6	
A	50	1,155	1,202	1,315	1,217	−2.4	
B	43	1,009	1,050	1,138	990	−2.5	
BD1354[a]	46	1,066	1,114	1,213	160	−3.0	−3.4
Namibian xenoliths							
1	47	11.5	1,071	1,156	1,092	−2.4	
20	42	996	1,006	990	1,000	−3.9	
34	38	1,001	1,021	1,010	960	−1.7	
1	37	946	881	1,000	935	−1.9	
6	46	1,082	1,090	1,208	1,204	−3.6	
Yakutian Xenoliths							
Uv-624	43	847	856	874	847	−2.7	
BD-2125	45	1,037	1,120	995	1,054	−1.9	
UV417/89[a]	50	974	955	963	850	−4.8	−4.4
UV61/91[a]	51	1,031	1,045	1,117	1,168	−3.8	−3.4

NG85, Grt–Opx barometer of Nickel and Green (1985) (in kbar); H84, Grt–Opx thermometer of Harley (1984); NW79, Grt–Ol thermometer of O'Neill and Wood (1979); Ai93, Grt–Cpx thermometer of Ai (1993); T98, Cpx–OPx thermometer of Taylor (1998) (in °C). $\Delta log(f_{O_2})_1$, calculated values by garnet–clinopyroxene–silica barometer relative to the QFM buffer of Frost (1991); $\Delta log(f_{O_2})_2$, calculated values by garnet–orthopyroxene–olivine barometer of Gudmundson and Wood (1995) relative to the QFM buffer. For f_{O_2} calculations P–T parameters obtained from garnet–orthopyroxene, thermobarometers of Harley (1984) and Nickel and Green (1985) were used. Analyses for the calculations were taken from: Carswell et al. (1979), Mitchell (1984), Pokhilenko et al. (1991), Sobolev et al. (1984)
[a] specimens with garnet Fe^{+3}/Σ Fe measured by the Mossbauer technique from Canil and O'Neil (1996) and McCammon and Kopylova (2004).

Appendix 2

Table 7 Eclogite garnet–clinopyroxene parageneses chosen for f_{O_2}calculations

Sample	EG79	P(kbar)	$(Si + Ti)_{Grt}$	$\%Fe^{+3}$	%Andr	$\Delta log(f_{O_2})$
Yakutian inclusions in diamonds						
M-734	1,267	45.0	3.02	4.85	2.35	−5.4
M-742	1,285	45.0	3.03	5.97	3.33	−4.0
M-636	1,085	45.0	3.04	5.03	3.18	−4.7
M-748	1,229	45.0	3.03	1.56	0.88	−5.8

Table 7 Eclogite garnet–clinopyroxene parageneses chosen for f_{O_2} calculations

Sample	EG79	P(kbar)	$(Si + Ti)_{Grt}$	$\%Fe^{+3}$	%Andr	$\Delta log(f_{O_2})$
M-422	1,085	45.0	3.05	4.56	2.60	−3.6
M-423	1,305	45.0	3.03	7.26	4.13	−2.4
M-46D	986	45.0	3.02	2.52	1.67	−3.0
U-41/3	1,140	45.0	3.02	7.47	5.04	−2.6
U-66/3	1,192	45.0	3.01	7.02	3.95	−3.2
Ud-4/90-1	1,132	45.0	3.03	4.72	2.87	−2.9
Ud-4/90-12-4	1,200	45.0	3.04	3.44	2.02	−4.1
Ud-4/90-13-6	1,138	45.0	3.03	3.68	2.22	−3.7
Ud-10/90-23	996	45.0	3.04	1.03	0.72	−6.0
South African and Guinea inclusions in diamonds						
P-3	1,310	50.0	3.04	3.98	1.61	−4.9
P-5	1,252	50.0	3.02	4.18	2.64	−4.5
P-18	1,336	50.0	3.02	9.18	4.14	−3.7
P-35	1,323	50.0	3.02	11.28	5.11	−1.3
P-38	1,266	50.0	3.01	0.96	0.40	−8.1
P-44	1,267	50.0	3.01	6.53	3.49	−4.8
P-45	1,364	50.0	3.02	6.22	3.36	−3.0
P-46	1,299	50.0	3.01	11.99	5.46	−1.2
P-47	1,305	50.0	3.03	1.91	0.97	−5.0
P-65	1,255	50.0	3.04	4.17	2.56	−4.0
P-66	1,208	50.0	3.01	4.65	2.70	−3.7
P-103	1,298	50.0	3.01	6.54	3.97	−3.7
P-104	1,289	50.0	3.01	11.36	5.22	−1.1
P-109	1,200	50.0	3.05	0.65	0.40	−7.9
P-113	1,332	50.0	3.04	5.42	2.48	−2.7
P-115	1,315	50.0	3.02	11.62	5.33	−1.7
RV-69	1,277	50.0	3.02	0.61	0.40	−8.1
KK-96	1,258	50.0	3.01	6.95	3.33	−3.5
7[a]	1,180	50.0		3.33	2.06	−4.2
20[a]	1,113	50.0		3.14	1.96	−2.5
41[a]	1,138	50.0		5.03	3.04	−3.0
Australian inclusions in diamonds						
A29	1,267	50.0	3.05	3.41	2.04	−3.3
A33	1,236	50.0	3.03	3.17	1.83	−3.8
A31	1,278	50.0	3.03	6.52	2.71	−1.4
Venezuela inclusions in diamonds						
Gm-54	1,103	50.0	3.03	2.61	1.48	−3.9
037c-a	1,188	50.0	3.03	3.12	1.62	−3.6
v-19	1,171	50.0	3.02	5.00	2.83	−3.1
Yakutian diamond-bearing xenoliths						
M-45	1,058	45.0	3.02	5.26	2.51	−4.7
M-46X	1,034	45.0	3.04	2.15	1.28	−4.0
M-52	1,020	45.0	3.03	6.54	3.82	−4.1
M-50	1,004	45.0	3.04	9.76	6.54	−7.1
M-49	1,015	45.0	3.03	1.43	0.76	−4.8
A-811	989	45.0	3.04	3.55	2.06	−2.2
M-54-R1	1,040	45.0	3.03	0.54	0.24	−5.6
BM-432	1,040	45.0	3.02	10.12	4.60	−0.6
U-464/86	994	45.0	3.01	5.51	4.08	−3.3
U-58/2	1,195	45.0	3.01	8.91	4.23	−2.5
U-55/2	1,074	45.0	3.01	10.30	4.21	−0.8
U-8/1	1,271	45.0	3.01	10.70	4.53	−2.9
Ud-76/2	1,236	45.0	3.04	4.70	2.08	−4.4
Ud-92/2	1,235	45.0	3.05	2.07	0.83	−5.1
Ud-59/2	1,198	45.0	3.02	4.59	1.47	−1.5
Ud-28	1,192	45.0	3.02	3.67	2.56	−2.8
M-85	1,077	45.0	3.03	1.71	1.03	−4.5
M-2110	1,090	45.0	3.04	2.01	1.28	−4.8
M-63	974	45.0	3.02	0.77	0.38	−5.7
236[a]	1,007	45.0		10.65	3.71	−2.3
281/2[a]	1,098	45.0		19.94	7.40	−2.7
African diamond-bearing xenoliths						
6	1,136	45.0	3.02	3.84	1.09	−1.9
17	1,700	45.0	3.02	6.10	2.12	−1.5
18	1.191	45.0	3.02	6.10	2.12	−0.6
19	1,297	45.0	3.02	4.55	1.68	1.1
XM26	1,178	45.0	3.01	6.16	3.03	−2.4

Table 7 Eclogite garnet–clinopyroxene parageneses chosen for f_{O_2} calculations

Sample	EG79	*P*(kbar)	$(Si+Ti)_{Grt}$	$\%Fe^{+3}$	%Andr	$\Delta log(f_{O_2})$
JJG891	1,359	45.0	3.02	0.55	0.21	−7.3
KEC-86-DB-9	1,344	45.0	3.04	9.12	4.30	−1.7
Finnish diamond-bearing xenoliths						
L-78	1,275	45.0	3.02	15.14	4.21	−3.6
L-80	1,248	45.0	3.01	8.36	3.31	−3.0
SEI-4	1,187	45.0	3.01	2.96	0.82	−3.6
African xenoliths						
6913-5	1,113	45.0	3.01	4.79	2.16	−2.6
6913-10	1,128	45.0	3.02	8.83	3.79	−0.1
2	1,444	45.0	3.01	4.46	1.24	−1.1
4	1,196	45.0	3.03	4.36	1.21	−2.6
1	1,164	45.0	3.03	0.62	0.27	−7.4
4	1,114	45.0	3.03	3.75	2.02	−6.7
5	1,145	45.0	3.02	1.97	1.03	−7.5
8	1,066	45.0	3.02	4.98	2.96	−3.2
K-3	1,118	45.0	3.02	6.18	3.02	−4.2
K-4	1,131	45.0	3.03	5.85	3.41	−5.1
K-5	1,159	45.0	3.4	8.36	4.78	−8.0
SRV1	1,143	45.0	3.03	2.16	0.69	−1.8
R-7	1,104	45.0	3.02	6.08	3.00	−0.5
R-8A	993	45.0	3.03	10.63	3.13	−2.0
R-22	1,063	45.0	3.02	13.19	9.39	−2.1
R-35	1,260	45.0	3.02	4.19	1.70	−1.0
R-51B	1,103	45.0	3.05	6.56	3.38	−4.1
R-71	1,042	45.0	3.01	3.52	1.31	−5.3
R-76A	1,242	45.0	3.02	4.64	1.96	−3.8
R-76B	1,256	45.0	3.03	4.34	1.77	−5.4
K-86-GB-70	934	45.0	3.03	0.45	0.29	−8.4
K-86-KB-3	1,035	45.0	3.02	11.28	4.17	0.1z
K-86-KB-74B	960	45.0	3.02	6.03	2.74	0.0
KG-86-76	978	45.0	3.01	6.03	3.72	−3.2
K-86-11	934	45.0	3.03	0.51	0.25	−5.4
K-86-72A	944	45.0	3.01	4.87	3.60	1.3
K-86-72B	1,004	45.0	3.02	6.97	4.85	−1.6
K-86-2	1,010	45.0	3.01	5.03	1.89	−2.4
K-86-58	923	45.0	3.03	11.63	2.56	−2.6
K-86-73A	1,070	45.0	3.03	6.20	2.19	−3.8
K-86-73B	977	45.0	3.01	10.81	3.83	−3.3
K-86-90	1,067	45.0	3.03	9.07	3.38	−2.5
K-86-107	1,086	45.0	3.03	7.47	1.67	−0.9
K-81-12	935	45.0	3.02	3.92	3.30	−4.3
K-81-21	1,048	45.0	3.01	3.55	2.14	−3.7

$(\%Fe^{+3} - 100*Fe^{+3})/(Fe^{+3} + Fe^{+2})$ in the garnets; %Andr, percent of andradite component; $(Si+Ti)_{Grt}$, silica and titan content in the garnet (in f.u.); EG79, thermometers of Ellis and Green (1979); *P*, pressure in kbar; $\Delta \log(f_{O2})$, calculated values by garnet–clinopyroxene–silica barometer relative to the QFM buffer of Frost (1991). Analyses for the calculations were taken from: Beard et al. (1996), Gurney et al. (1985), Hills and Haggerty (1989), Harte and Gurney (1975), Jaques et al. (1989), Jerde et al. (1993), Kaminsky et al. (2000), Kushiro and Aoki (1968), Lappin and Dawson (1975), MacGgregor and Manton (1986), O'Hara et al. (1975), Reid et al. (1976), Safronov et al. (1980), Smyth and Hatton (1977), Sobolev (1977), Sobolev et al. (1983, 1998), Spetsius et al. (1992), Stachel et al. (2000), Taylor et al. (1996)

[a] specimens with garnet and clinopyroxene; Fe^{+3}/Σ Fe Mossbauer taken from McCammon et al. (1998) and Sobolev et al. (1999b)

References

Ai Y (1993) A revision of the garnet–clinopyroxene Fe^{+2}–Mg exchange geothermometer. Contrib Mineral Petrol 115:467–473

Aranovich L Ya (1991) Mineral equilibrium of the multicomponent solid solutions. Moscow, 253pp (in Russian)

Ballhaus C (1993) Redox states of lithospheric and asthenospheric upper mantle. Contrib Mineral Petrol 114:331–348

Ballhaus C, Frost BR (1994) The generation of oxidized CO_2-bearing basaltic melts from reduced CH_4-bearing upper mantle sources. Geochim Cosmochim Acta 58:4931–4940

Ballhaus C, Berry RF, Green DH (1991) High pressure experimental calibration of the olivine–orthopyroxene–spinel oxygen geobarometer: implications for the oxidation state of the upper mantle. Contrib Mineral Petrol 107:27–40

Beard LB, Fraracci KN, Taylor LA, Snyder GA, Clayton RA, Mayeda TK, Sobolev NV (1996) Petrography and geochemistry of eclogites from the Mir kimberlite, Yakutia, Russia. Contrib Mineral Petrol 125:293–310

Belonoshko A, Saxena SK (1992) A unified equation of state for C–H–O–N–S–Ar composition and their mixtures up to very high temperatures and pressures. Geochim Cosmochim Acta 56:3611–3626

Bulanova GP, Pavlova LP (1987) Association of magnesite peridotite in diamond from pipe Mir. Dokl Akad Nauk SSSR 295:1452–1456 (in Russian)

Bulanova GP, Zayakina NV (1991) Mineralogical association of graphite–iron–cohenite in central region of diamond from pipe by name XXIII party congress. Dokl Akad Nauk SSSR 317:706–709 (in Russian)

Canil D, O'Neill HSC (1996) Distribution of ferric iron in some upper-mantle assemblages. J Petrol 37:609–635

Carswell DA, Clarke DB, Mitchell RH (1979) The petrology and geochemistry of ultramafic nodules from pipe 200, Northern Lesotho. In: Boyd FR, Meyer OA (eds) Proceedings of the second international kimberlite conference. Am Geophys Union 1:127–144

Christie DM, Carmichael ISE, Langmuir CH (1986) Oxidation states of mid-ocean ridge basalt glasses. Earth Planet Sci Lett 79:397–411

Dal Negro A, Carbonin S, Molin GM, Gundari AEH (1982) Incrystalline cation distribution in natural clinopyroxenes of tholeitic, transitional, and alkaline basaltic rocks. Adv Phys Geochem 2:117–150

Deines P, Harris JW, Gurney JJ (1987) Carbon isotopic composition, nitrogen content and inclusion composition of diamonds from the Roberts Victor kimberlite, South Africa: evidence for $\delta^{13}C$ depletion in the mantle. Geochim Cosmochim Acta 51:1227–1243

Deines P, Harris JW, Spear PM, Gurney JJ (1989) Nitrogen and $\delta^{13}C$ content of finsh and premier diamonds and their implications. Geochim Cosmochim Acta 53:1367–1378

Ellis DJ, Green DH (1979) An experimental study of the effect of Ca upon garnet–clinopyroxene Fe–Mg exchange equilibria. Contrib Mineral Petrol 71:13–22

Frost BR (1991) Introduction to oxygen fugacity and its petrological importance. Rev Miner 25:1–9

Galimov EM (1984) Isotopic composition variations and their connection with diamond genesis. Geochimiya 8:1091–1117 (in Russian)

Giardini AA, Melton CE (1975) Gases released from natural and synthesis diamonds by crushing under high vacuum at 200°C, and their significance to diamond genesis. Fortschr Miner Spec Iss 52:455–464

Girnis A, Grutter H (2003) Thermobarometry of mantle peridotites: calibration based on experimental and natural data. Eighth international kimberlite conference, Victoriya [Extended Abstr]

Gudmundson G, Wood BJ (1995) Experimental tests of garnet peridotite oxygen barometry. Contrib Mineral Petrol 119:56–67

Gurney JJ, Harris IW, Rickard RS, Moore RO (1985) Inclusions in premier mine diamonds. Trans Geol Soc S Afr 88:301–310

Haggerty SE (1986) Diamond in a multy-constrained model. Nature 320:34–38

Haggerty SE, Tompkins LA (1983) Redox state of earth's upper mantle from kimberlitic ilmenites. Nature 303:295–300

Hansen EC, Newton RC, Janardan AS (1984a) Pressure, temperatures and metamorphic fluids across an unbroken amfibolite facies to granulite facies transition in Southern Karnataka, Indian. In: Kroner A, Hanson GN, Goodwin AM (eds) Archean geochemistry. The origin and evolution of the archean continental crust. Springer-Verlag, Berlin, pp161–181

Hansen EC, Newton RC, Janardhan AS (1984b) Fluid in clusions in rock from the amphibolite-facies gneiss to charnokite progression in southern Karnataka, India direct evidence concerning the fluids of granulite metamorphism. J Metam Geol 2:249–264

Harley SL (1984) An experimental study of the partitioning of the Fe and Mg between garnet and orthopyroxene. Contrib Mineral Petrol 86:359–373

Harte B, Gurney JJ (1975) Evolution of clinopyroxene and garnet in an eclogite nodules from the Roberts Victor kimberlite pipe, South Africa. Phys Chem Earth 9:367–387

Hills DV, Haggerty SE (1989) Petrochemistry of eclogites from Koidu kimberlite complex, Sierra Leone. Contrib Mineral Petrol 103:397–422

Janardan AS, Newton RC, Hansen EC (1982) The transformation of amphibole facies gneiss to charnokite on Southern Karnataka and Northern Tamil Nadu, India. Contrib Mineral Petrol 79:130–149

Jaques AL, Hall AE, Sheraton JW, Smith CB, Sun S-S, Drew RM, Foundolis C, Ellingsen K (1989) Composition of crystal inclusions and C isotopic composition of argyle and ellendale diamonds. In: Kimberlites and related rocks. Proceedings of the fourth international kimberlite conference GSA. Spec Public N 14(2):966–989

Jerde EA, Taylor LA, Crozaz G, Sobolev NV (1993) Diamondiferous eclogites from Yakutia, Siberia: evidence for a diversity of protoliths. Contrib Mineral Petrol 114:189–202

Johnston CA, Essene EJ (1982) The formation of garnet in olivine-bearing metagabbros from the Andirocdacks. Contrib Mineral Petrol 8:240–251

Kaminsky FV, Zakharchenko OD, Griffin WL, Der Channer DM, Khachatryan GK (2000) Diamonds from the Guaniamo area, Venezuela. Can Miner 38:1347–1370

Kushiro I, Aoki KI (1968) Origin of some eclogite inclusions in kimberlite. Am Min 53:1347–1367

Kuskov OL, Fabrichnaya OB (1990) Phase relationships in the system FeO–MgO–SiO_2 on the boundary of the upper mantle and transitional zone. Geochimiya 2:266–278 (in Russian)

Lamb W, Valley JW (1984) Metamorphism of granulites in low-CO_2 vapor-free environment. Nature 312:56–58

Lappin MA, Dawson JB (1975) Roberts Victor cumulate eclogites and their re-equilibration. Phys Chem Earth 9:351–365

Lindsley DH (1981) The formation of pigeonite on the join hedenbergite-ferrosilite at 11.5 and 15 kbar: experiments and a solution model. Am Miner 66:1175–1182

Lindsley DH, Grover JE, Davidson PM (1981) The thermodynamics of the $Mg_2Si_2O_6$–$CaMgSi_2O_6$ join: a review and an improved model. Adv Phys Geochem 1:149–175

Luth RW, Virgo D, Boyd FR, Wood BJ (1990) Ferric iron in mantle-derived garnets. Implications for thermobarometry and for the oxidation state of the mantle. Contrib Mineral Petrol 104:56–72

MacGregor ID, Manton WI (1986) Roberts Victor eclogites: ancient oceanic crust. J Geophys Res 91:14063–14079

McCammon CA, Kopylova MG (2004) A redox profile of the slave mantle oxygen fugacity control in the cratonic mantle. Contrib Mineral Petrol 148:55–68

McCammon CA, Chinn IL, Gurney JJ, McCallum ME (1998) Ferric iron content of mineral inclusions in diamonds from George Creek, Colorado determined using Mossbauer spectroscopy. Contrib Mineral Petrol 133:30–37

Messiga B, Scambelluri M (1991) Retrograde P-T-t path for the Voltri Massif eclogites (Ligurian Alps, Italy): some tectonic implications. J Metam Geol 9:93–109

Mitchell RH (1984) Garnet lherzolites from the Hanaus-Land Lourensia kimberlites of Namibia. Contrib Mineral Petrol 86:178–188

Mitchell RH (1991) Kimberlites and lamproites: primary sources of diamond. Geosci Can 18:1–16

Moecher DP, Essene EL, Anovitz LM (1988) Calculation and application of clinopyroxene–garnet–plagioclase–quartz geobarometers. Contrib Mineral Petrol 100:92–106

Mottana A, Church WR, Edgar AD (1968) Chemistry, mineralogy and petrology of an eclogite from the type locality (Saulpa, Austria). Contrib Mineral Petrol 18:338–346

Mukhopadhyay B (1991) Garnet–clinopyroxene geobarometry. The problems, prospects and an approximate solution with some applications. Am Miner 76:512–529

Nakamura D, Banno S (1997) Thermodynamic modeling of sodic pyroxene solid-solution and its application in a garnet–omphacite–kyanite–coesite geothermobarometer for UHP metamorphic rocks. Contrib Mineral Petrol 130:93–102

Nickel KG, Green DH (1985) Empirical geothermobarometry for garnet peridotite and implications for the nature of the lithosphere, kimberlites and diamonds. Earth Planet Sci Lett 73:158–170

O'Hara MJ, Saunders MJ, Mercy ELP (1975) Garnet peridotite, possible ultrabasic magmas and eclogite: interpretation of upper mantle processes in kimberlite. Phys Chem Earth 9:571–604

O'Neill HS, Wall VJ (1987) The olivine–orthopyroxene–spinel oxygen barometer, the nickel precipitation curve, and the oxygen fugacity of the earth's upper mantle. J Petrol 28:1169–1191

O'Neill HS, Wood BJ (1979) An experimental study of Fe–Mg partitioning between garnet and olivine and its calibration as a geothermometer. Contrib Mineral Petrol 70:59–70

Pal'yanov YuN, Sokol AG, Borzdov YuM, Khokhryakov AF, Sobolev NV (1999). Diamond formation from mantle carbonate fluids. Nature 400:417–418

Perchuk AL, Aranovich L Ya (1991) Thermodynamic of jadeite–hedenbergite solid solution. Geochimiya 4:539–547 (in Russian)

Pokhilenko NP, Tomilenko AA (2001) Fluid composition in the upper mantle rocks. In: Twelfth Russian conference Exper Miner, Chern, p276

Pokhilenko NP, Pearson DG, Boyd FR, Sobolev NV (1991) Megacrystalline dunite and peridotites: host for Siberian diamonds. Carnegie Inst Wash Yearb 90:11–23

Reid AM, Brown RW, Dawson IB, Whittfeld GG, Siebert IC (1976) Garnet and pyroxene composition in some diamondiferous eclogites. Contrib Mineral Petrol 58:203–206

Richardson SH, Harris JW, Gurney JJ (1993) Three generation of diamonds from old continental mantle. Nature 366:256–258

Ryabchikov ID, Brey GP, Bulatov VK (1993) Near solidus melts in carbonated peridotites at 50 kbars. In: Bogatikov OA (ed) Rift and pold belt magmatism. Nauka, Moscow, pp265–274 (in Russian)

Safronov AF, Nikishov KN, Botkunov AI, Gotovtsev VV, Mahotko VF (1980) Composition of garnets and pyroxenes from diamond-bearing eclogites from pipes Mir and Udachnaya. Sov Geol Geophys 21:76–82

Saxena SK (1989) Oxidation state of the mantle. Geochim Cosmochim Acta 53:89–95

Schrauder M, Navon O (1993) Solid carbon dioxide in a natural diamond. Nature 365:42–44

Schumaher JC (1991) Empirical ferric iron corrections: necessity, assumption, and effects on selected geothermobarometers. Mineral Mag 55:3–18

Seckendorff V, O'Neill HSC (1993) An experimental study of Fe–Mg partitioning between olivine and orthopyroxene at 1173, 1273 and 1423K and 1.6 GPA. Contrib Mineral Petrol 113:196–207

Simakov SK (1993) Garnet–clinopyroxene oxygen barometer for mantle eclogites. Dokl Akad Nauk R 332:83–84 (in Russian)

Simakov SK (1998) Redox state of earth's upper mantle peridotites under the ancient cratons and it connection with diamond genesis. Geochim Cosmochim Acta 62:1811–1820

Simakov SK (2005) Clinopyroxene barometry of mantle eclogite xenoliths and the application for assessment of diamond potential. Dokl Earth Sci 400:113–115

Simakov SK, Taylor LA (2000) Geobarometry for deep mantle eclogites: solubility of Ca-Tschermaks in clinopyroxene. Inter Geol Rev 42:534–544

Smyth JR, Hatton CJ (1977) A coesite-sanidine grospydite from the Roberts Victor kimberlite. Earth Planet Sci Lett 34:284–290

Sobolev NV (1977) Deep-seated inclusions in kimberlites and the problem of the composition of the upper mantle. American Geophysical Union, Washington p 278

Sobolev EV, Lenskaya SV, Lisoyvan VI (1966) Some physical properties of diamonds of Yakutian eclogite. Dokl Akad Nauk SSSR 168:1151–1153 (in Russian)

Sobolev NV, Yefimova ES, Usova LV (1983) Diamond eclogite paragenesis of kimberlite pipe Mir. In: Sobolev NV, Vasiliev UR, Kepezhinskas VV (eds) Deep xenoliths and problems of upper mantle petrology. Novosibirsk, pp4–16 (in Russian)

Sobolev NV, Pokhilenko NP, Efimova ES (1984) Xenoliths of diamond-bearing peridotites in kimberlites and the problem of diamond origin. Sov Geol Geophys 25:62–76

Sobolev NV, Taylor LA, Zuev VM, Bezborodov SM, Snyder GA, Sobolev VN, Yefimova ES (1998) The specific features of eclogitic paragenesis of diamonds from Mir and Udachnaya kimberlite pipes (Yakutia). Sov Geol Geophys 39:1667–1678

Sobolev NV, Sobolev VN, Snyder GA, Yefimova ES, Taylor LA (1999a) Significance of eclogitic and related parageneses of natural diamonds. Int Geol Rev 41:129–140

Sobolev VN, McCammon CA, Taylor LA, Snyder GA, Sobolev NV (1999b) Precise Mossbauer milliprobe determination of ferric iron in rock-forming minerals and limitations of electron microprobe analysis. Am Mineral 84:78–85

Sobolev NV, Fursenko BA, Goryainov SV, Shu J, Hemley RJ, Mao HK, Boyd FR (2000) Fossilized high pressure from the earth's deep interior: the coesite-in-diamond barometer. Proc Natl Acad Sci USA 97:11875–11879

Spear FS, Markussen JC (1997) Mineral zoning, P-T-X-M phase relations, and metamorphic evolution of some Andirondack granulites, New York. J Petrol 38:757–783

Spetsius ZV, Bulanova GP, Griffin VL (1992) Diamond-bearing eclogite with garnet inclusion in diamond from pipe Mir. Dokl Akad Nauk R 322:134–137 (in Russian)

Stachel T, Brey GP, Harris JW (2000) Kankan diamonds (Guinea). I: from the lithosphere down to the transition zone. Contrib Mineral Petrol 140:1–15

Taylor WR (1998) An experimental test of some geothermometer and geobarometer formulations for upper mantle peridotites with application to the thermobarometry of fertile lherzolite and garnet websterite. N Jb Miner Abh 172:381–408

Taylor WR, Green DH (1989) The role of reduced C–O–H fluids in mantle partial melting. In: Ross JR (ed) Kimberlites and related rocks. Proceedings of the fourth international kimberlite conference 1:592–602

Taylor WR, Green DH (1991) Mineral chemistry of silicate and oxide phases from fertile peridotite equilibrated with a C–O–H fluid phase—a low f_{O_2} data set for the calculation of mineral barometers, thermometers and oxygen sensors. Fifth international kimblite conference abstract, pp417–419

Taylor LA, Snyder GA, Crozaz G, Sobolev VN, Yefimova ES, Sobolev NV (1996) Eclogite inclusions in diamonds—evidence of complex mantle processes over time. Earth Planet Sci Lett 142:535–551

Ulmer GC, Grandstaff DE, Weiss D, Moats MA, Buntin TJ, Gold DP, Hatton CJ, Kadik A, Koseluk RA, Rosenhauer M (1987) The mantle redox state; an unfinished story? Mantle metasomatism and alkaline magmatism. Spec Pap Geol Soc Am 215:5–23

Woermann E, Rosenhauer M (1985) Fluid phases and redox state of the earth's mantle. Extrapolations based on experimental, phase theoretical and petrological data. Fortschr Miner 63:263–349

Wood BJ, Banno S (1973) Garnet–orthopyroxene and orthopyroxene–clinopyroxene relationships in simple and complex systems. Contrib Mineral Petrol 42:109–124

Wood BJ, Nickols J (1978) The thermodynamic properties of reciprocal solid solutions. Contrib Mineral Petrol 66:389–400

Woodland AB, Koch M (2003) Variation in oxygen fugacity with depth in the upper mantle beneath the Kaapvaal craton, Southern Africa. Earth Planet Sci Lett 214:295–310

Woodland AB, O'Neill HSC (1993) Synthesis and stability of $Fe_3Fe_2Si_3O_{12}$ garnet and phase relations with $Fe_3Al_2Si_3O_{12}$-$Fe_3Fe_2Si_3O_{12}$ solutions. Am Miner 78:1002–1015

Woodland AB, Peltonen (1999) Ferric iron contents of garnet and clinopyroxene and estimated oxygen fugacities of peridotite xenoliths from the fastern Finland kimberlite province. In: Gurney JJ, Gurney LG, Pascal MD, Richardson SH (eds) Proceedings of the seventh international kimberlite conference 2:904–911

Wyllie PJ (1977) Mantle fluid compositions buffered by carbonates in peridotite-CO_2–H_2O. J Geol 85:187–207

Yaxley GM (1999) Phase relations of carbonated eclogite under upper mantle PT conditions—implications for carbonatite petrogenesis. In: Gurney JJ, Gurney LG, Pascal MD, Richardson SH (eds) Proceedings of the fourth international kimberlite conference 2:933–939

Zhang Z, Saxena SK (1991) Thermodynamic properties of andradite and application to skarn with coexisting andradite and hedenbergite. Contrib Mineral Petrol 107:255–263